

Enhanced charge extraction in inverted hybrid photovoltaic cells assisted by graphene nanoflakes†

Yun-Ming Sung,^a Fang-Chi Hsu,^{*b} Di-Yan Wang,^c I.-Sheng Wang,^c Chia-Chun Chen,^{cd} Hsueh-Chung Liao,^e Wei-Fang Su^e and Yang-Fang Chen^{*a}

Received 7th June 2011, Accepted 30th August 2011

DOI: 10.1039/c1jm12571k

We use graphene nanoflakes (GNFs) to greatly enhance the charge extraction out of a photoactive blend in inverted hybrid poly(3-hexylthiophene):(6,6)-phenyl C₆₁ butyric acid methyl ester (P3HT:PCBM)/ZnO-nanorod photovoltaic cells. Instead of a continuous film, solution processed GNFs with dimensions less than 200 nm × 200 nm are homogeneously scattered on top of the well-aligned ZnO-nanorods. Those GNFs play key roles, they serve as an electron drain to collect electron flow out to ZnO-nanorods, enhance the carrier mobility of the device and promote holes to drift toward the surface in contact with the cathode. As a result, there is a large enhancement in photocurrent and photovoltage of 35% and 27%, respectively, leading to an improved cell efficiency by up to about 100%.

Introduction

Graphene, a class of new 2D crystals, has gained great attention in the fields of materials science and condensed matter physics recently. Due to its exceptionally high carrier mobility¹ and high conductivity,² the merging of graphene into electronics applications is underway. Successful use of graphene/graphene oxide as an active component in a field effect transistor,^{3,4} an anode in a dye-sensitized² or an organic solar cell,⁵ and an acceptor in an organic photovoltaic device⁶ has been demonstrated.

Inverted photovoltaic cell configuration incorporating an inorganic semiconductor and a high work function electrode overcomes the stability problems of the conventional cells such as the corrosion of poly(3,4-ethylene dioxythiophene):poly(styrene sulfonate) (PEDOT:PSS) on indium-tin oxide (ITO) due to its acidic nature^{7,8} and the oxidation of Al electrode upon exposure to air. ZnO is an environmental friendly low-cost semiconducting material and can be made in various forms with low temperature simple processing methods. Utilizing nanostructured ZnO in the form of nanorods^{9–11} and nano-ridges¹² in inverted photovoltaic cells enlarges the charge carrier collection

surface and offers ordered carrier transport pathways.¹³ Poly(3-hexylthiophene):(6,6)-phenyl C₆₁ butyric acid methyl ester (P3HT:PCBM) blend is the most prominent photoactive material used in the inverted device structure as in the conventional one. In inverted hybrid polymer blend/nanorod cells, the photoactive layer thickness is typically more than 300 nm,^{9–11} which is almost double the height of the embedded inorganic nanostructure. Excitons generated among the nanorods can be split and then collected at the metal oxide surface within their diffusion length. However, for those above the nanorods, charge recombination before reaching the metal oxide is unavoidable for the long transport pathways (>100 nm). Though the use of a thick photoactive layer absorbs greater than 95% of the incident light over the wavelength range of 450–600 nm,¹⁴ which in turn enhances the power conversion efficiency,^{15,16} the carrier loss in the thick film limits the collected charge flows. Therefore, it is essential and critical to effectively extract charges out of the excess photoactive layer while the photon absorption capability is enhanced.

Herein, we provide an alternative solution to overcome the above difficulty by introducing graphene nanoflakes (GNFs) into the hybrid P3HT:PCBM/ZnO photovoltaic cells. It is found that the presence of GNFs largely enhances the cell efficiency by about 100%. Instead of a continuous film, incomplete coverage of the ZnO-nanorod growth surface by GNFs is able to lead to large increments in photocurrent and open circuit voltage. Those GNFs are spatially isolated from each other and each forms a three-dimensional electron potential well with the surrounding polymer blend. The built-in electric field drives the photo-generated electron flows to go through those conducting flakes to reach the ITO electrode. The electron transport path thus becomes more well-defined and is of lower resistivity leading to enhanced carrier mobility. Additionally, a relatively higher

^aDepartment of Physics, National Taiwan University, Taipei, 106, Taiwan. E-mail: yfchen@phys.ntu.edu.tw

^bDepartment of Materials Science and Engineering, National United University, Miaoli, 360, Taiwan. E-mail: fangchi@nuu.edu.tw

^cDepartment of Chemistry, National Taiwan Normal University, Taipei, 106, Taiwan

^dInstitute of Atomic and Molecular Science, Academia Sinica, Taipei, 106, Taiwan

^eDepartment of Materials Science and Engineering, National Taiwan University, Taipei, 106, Taiwan

† Electronic supplementary information (ESI) available: Performance of devices with various GNF concentrations and AFM morphology data. See DOI: 10.1039/c1jm12571k

concentration of photogenerated holes reaches the surface in contact with the cathode revealing the reduced intermolecular recombination due to improved electron mobility. Consequently, a larger amount of photogenerated carriers is extracted out resulting in improved photovoltaic cell performance.

Experimental details

Materials preparation

P3HT and PCBM were purchased from Lum Tec Co. Ltd (Taiwan) and used as received. The polymer blend solution was formed by mixing 25 mg P3HT ($M_w = 40$ kDa, PDI = 1.3, RR = 99.5%) and 15 mg PCBM in 1 mL dichlorobenzene solvent. The whole solution was stirred at 1000 rpm for one day. The GNF solution was prepared by exfoliation of graphite in surfactant–water solutions according to ref. 17 and used after passing through a 0.22 μm filter. The oriented ZnO-nanorods are grown vertically to the indium-tin-oxide (ITO) coated glass substrate by using the hydrothermal method.^{18,19} A 30 nm ZnO seed layer was spin-coated onto the patterned indium tin oxide (ITO) coated glass from a 0.35 M solution of zinc acetate dihydrate (Ridel-de Hagën) in the mixed solvents of monoethanolamine (Merck) and 2-methoxyethanol (Acros)¹⁸ at a rate of 3000 rpm. The film was then annealed at 200 °C for an hour to remove the residual organic solvents. The oriented ZnO-nanorod arrays were subsequently grown from the ZnO seed-coated substrates suspended in an aqueous solution of 35 mM zinc nitrate (Acros, 98% purity) and 35 mM hexamethylenetetramine (Acros) at 90 °C for 70 min in an oven.¹⁹ The preparation of the aligned ZnO-nanorod arrays was finished by dipping the substrate into deionized water to remove the residual salts and dried in N_2 gas flow. The resulting ZnO-nanorod length is ~ 120 nm.

Sample fabrication

Photovoltaic cells were fabricated based on the oriented ZnO-nanorod arrays. Initially, graphene sol–gel solution (5 mg mL^{-1}) after passing through the 0.22 μm filter was spin-coated onto the ZnO-nanorod arrays at a rate of 3000 rpm for 30 seconds. The whole structure was subsequently annealed at 180 °C for 4 min to remove the residual surfactant followed by the deposition of the P3HT:PCBM photoactive layer from *o*-dichlorobenzene solution at a spin rate of 400 rpm. After one day drying in air, the thickness of the resulting photoactive layer is in the range of 590–680 nm. Finally, a silver layer (~ 100 nm) was deposited thermally on top of the photoactive layer to complete the ZnO/GNFs/P3HT:PCBM/Ag photovoltaic devices. Typical active areas for photovoltaic devices are 3.0 mm^2 . Samples for UV-vis and Kelvin probe force microscopy (KFM) measurements have the same fabrication procedures as photovoltaic devices without metal deposition.

Characterization details

The current–voltage characteristics of the finished photovoltaic devices were evaluated by using a Keithley Model 2400 source meter under an illumination intensity of 100 mW cm^{-2} from a solar simulator (Newport Inc.) with an AM 1.5G filter. The UV-visible absorption spectroscopy was performed by using

a JASCO Model V-630 UV-vis spectrophotometer. The charge extraction in a linearly increasing voltage (CELIV) technique was performed in the dark by using a Textronic Model AFG3101 function generator to apply voltage pulses from -0.4 to 3 V and back to -0.4 V and the dynamic response of mobile carrier extraction was recorded simultaneously from a load of 83 Ω resistor in series to the photovoltaic cell by an Agilent Model DS05054A oscilloscope. Kelvin probe force microscopy (KFM) measurements were conducted in the dark and under illumination of a halogen lamp (Royal Philips Electronics, 139, 50 W) by using the Veeco Instruments Multimode AFM with an extender electronics module operating in the lift mode (typical lift height 20 nm) by a silicon cantilever with a PtIr surface coating. All characterizations are performed in air.

Results and discussion

Fig. 1(a) shows the top view field emission scanning electron microscopy (FESEM) image of graphene nano-flakes (GNFs) on oriented ZnO-nanorods. The hexagons are the ZnO-nanorods with a diameter of ~ 30 nm and the semitransparent nano-sheets (marked by red arrows) are GNFs. Since the nano-flakes are less than 200 nm \times 200 nm, those flakes can stand on top of ZnO nanorods with 30–40 nm rod-to-rod spacing. The distribution of GNFs on ZnO-nanorod arrays exhibits discontinuous but homogeneous arrangement (Fig. 1(b)). There is approximately 10% coverage of the ZnO-nanorod growth area by GNFs. After the subsequent polymer blend infiltration and a layer of silver metal deposition steps on the GNFs/ZnO structure, the photovoltaic cell is completed as the schematic device configuration shown in Fig. 1(c).

Fig. 2 presents the current(J)–voltage(V) characteristics of photovoltaic devices before (standard) and after GNF deposition under an illumination intensity of 100 mW cm^{-2} . The performance of the standard device yields a short circuit current (J_{SC}) of 7.5 mA cm^{-2} , an open circuit voltage (V_{OC}) of 0.44 V, a fill factor (FF) of 0.38, and a power conversion efficiency (PCE) of 1.26%. After incorporating GNFs, a remarkable enhanced device performance with a J_{SC} of 10.1 mA cm^{-2} , V_{OC} of 0.56 V, FF of

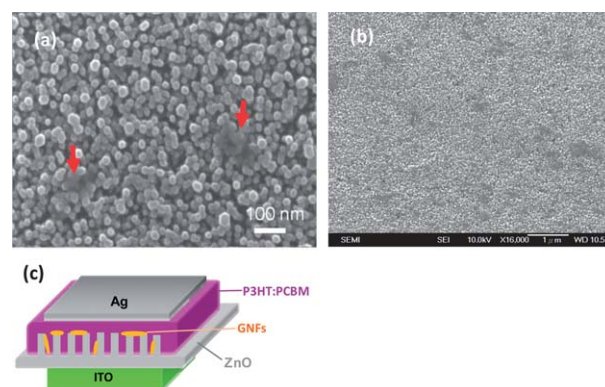


Fig. 1 Morphology of GNFs/ZnO structure and illustration of device configuration. (a) Top view FESEM image of GNFs on well aligned ZnO-nanorod arrays grown on the ITO coated glass substrate and (b) the distribution of GNFs on ZnO-nanorod arrays. (c) The schematic configuration of the ITO/ZnO/GNFs/P3HT:PCBM/Ag device.

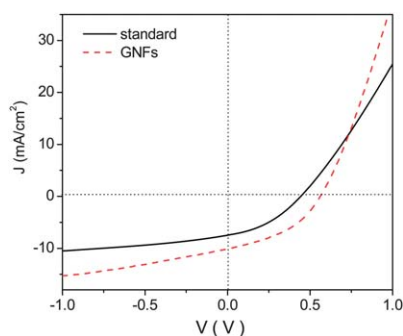


Fig. 2 Current–voltage characteristics of standard and GNF-modified photovoltaic cells under one Sun illumination with an AM 1.5G filter.

0.41, and PCE of 2.33% is obtained. Apparently, the performance enhancement comes from the large improvement in both J_{SC} and V_{OC} . Approximately 35% and 27% increments in J_{SC} and V_{OC} , respectively, are achieved for the best performance obtained.

We have tried to fabricate devices with various GNF concentrations and found out that PCEs for devices with GNF modification are enhanced (ESI†, Fig. S1 and Table S1). In this article, we focus on the case of optimal concentration for studying the mechanism. Moreover, the device performance varies from batch to batch and the variation is controlled within 10% based on 12 devices for each type. For the similar rod length used as this study, the reported¹³ PCE is $\sim 2\%$ for devices of 414 nm thick active layer and >30 nm thick seed layer. Our standard device has lower PCE because of a much thicker active layer (~ 600 nm) and a slightly thinner seed layer (~ 30 nm) used. The hole blocking effect is reduced for the thin seed layer and additional series resistance could lower the photocurrent in the case of thicker photoactive layer.¹³ Comparing to the parameters for a good device as reported,¹³ there are still $\sim 16\%$ and $\sim 10\%$ increments in J_{SC} and V_{OC} , respectively, for the GNF-modified device here. Thus, the effects of GNFs on the polymer–ZnO nanorod interface are real, but could lead to moderate improvements if a good device served as a baseline.

We point out here that we do not compare the performance of our standard device with Huang *et al.*¹¹ because the additional KG5 filter used in their calibration effectively enhances the photon flux in the visible regime, which raises up J_{SC} .

Since the use of a small amount of GNFs at the polymer–ZnO interface leads to the noticeable improvement in solar energy conversion, GNFs play a critical role in enhancing the charge collection capability. A systematic study for identifying the function of GNFs is carried out in the following.

Fig. 3 shows UV-vis absorbance of ZnO-nanorod arrays, GNFs/ZnO, P3HT:PCBM/ZnO, and P3HT:PCBM/GNFs/ZnO structures in the wavelength range of 300–800 nm. The pristine ZnO-nanorod arrays show an absorption edge at 375 nm and the characteristics of the spectrum remain after GNF deposition. In the P3HT:PCBM/ZnO structure, there are three pronounced absorption peaks at 515, 550, and 600 nm, which correlate with the vibronic state transition of the P3HT molecule between π – π^* bands²⁰ due to the strong π – π interaction among polymer chains. The result indicates that P3HT is in a highly ordered state in the blend.^{16,21} As GNFs are introduced, the obtained spectrum

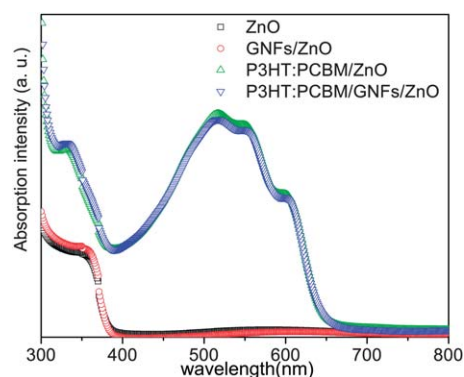


Fig. 3 UV-visible absorption spectra of ZnO, GNFs/ZnO, P3HT:PCBM/ZnO, and P3HT:PCBM/GNFs/ZnO structures.

shows negligible changes in both the optical density and features suggesting a similar volume of effective photoactive substance and nonapparent change of polymer chain ordering in an originally high crystalline order state. GNF, therefore, has no direct or indirect contribution to light absorption, which affects J_{SC} .

The charge extraction in a linearly increasing voltage (CELIV) technique^{22–24} was conducted in a dark environment to directly measure the carrier mobility of a photovoltaic cell. A reversed triangle-shaped pulse voltage bias was applied to the photovoltaic cell and the dynamic response of mobile carrier extraction was recorded simultaneously. By knowing the time for the extraction current reaching its maximum (t_{max}), the thickness of the photoactive layer (d), the capacitive displacement current ($j(t=0)$), and the maximum extraction current ($\Delta j(t=t_{max})$), the carrier mobility (μ) is then estimated²² using $\mu = 2d^2/[3t_{max}^2(1 + 0.36\Delta j(t=t_{max})/j(t=0))]$. In the present study, the voltage applied was from -0.4 to 3 V at a ramping rate of 0.225 V μs^{-1}

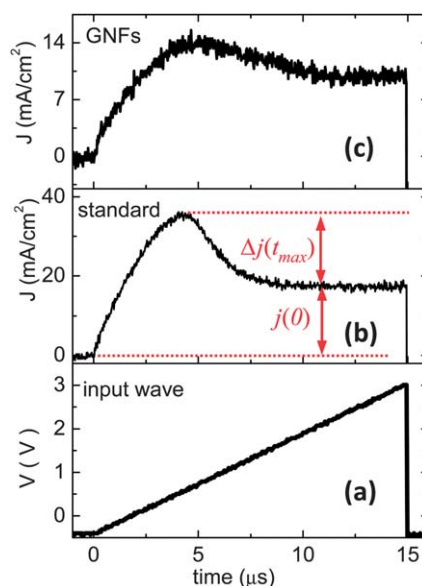


Fig. 4 CELIV measurements of photovoltaic cells in the dark. (a) Triangle-shaped voltage pulse with the application voltages from -0.4 to 3 V and back to -0.4 V. The corresponding charge extraction response for (b) standard (595 nm thick) and (c) GNF-modified (680 nm thick) devices.

and then back to -0.4 V (Fig. 4(a)). The corresponding charge extraction dynamic responses during the voltage ramping period were recorded for both types of devices accordingly (Fig. 4(b) and (c)). The device mobilities were calculated to be 2.6×10^{-4} (standard) and $5 \times 10^{-4} \text{ cm}^2 \text{ V}^{-1} \text{ s}^{-1}$ (GNFs-modified). In a blend system, the CELIV technique probes the mobility of more mobile species.²⁵ Huang *et al.*²⁶ reported that the electron and hole mobilities of the P3HT:PCBM film are similar ($\sim 10^{-4} \text{ cm}^2 \text{ V}^{-1} \text{ s}^{-1}$) for the ratio studied here. Later, Baumann *et al.*²⁷ pointed out that the electron mobility ($\sim 10^{-4} \text{ cm}^2 \text{ V}^{-1} \text{ s}^{-1}$) is 10-fold larger than the hole mobility of the blend. Thus, we assign the only carrier species detected here to be the electron.

Fig. 5 illustrates the atomic force microscopy (AFM) images of the polymer blend on ZnO-nanorod arrays and GNFs/ZnO structures. Apparently, the surface texture of the P3HT:PCBM layer changes from fiber-like (Fig. 5(a)) to granular-like structure (Fig. 5(b)) after GNF deposition. The r.m.s. surface roughnesses of the $20 \mu\text{m} \times 20 \mu\text{m}$ surface area are of 9.0 (standard) and 10.2 nm (GNF-modified). We used the surface-area calculation function in our AFM program and found out that there is $\sim 0.1\%$ more surface area of GNF modified film than the standard one. Thus, the rough surface effect can only be considered as a minor effect for the device improvement, not able to lead to $\sim 100\%$ increment in cell efficiency.

The GNF solution used was prepared in surfactant-water base. It is highly possible that there are residual surfactants on the ZnO-nanorod surface during processing. Both residual surfactants and GNFs presenting on the ZnO-nanorod surface can affect the surface morphology. By considering this point, we have no strong evidence showing the existence of surfactants on the ZnO-nanorod surface from the measured the UV-vis absorption spectrum (ESI†, Fig. S3). The result may be because the little amount of residual surfactants is below the instrument detectable limit. On the other hand, we also measure the morphology of the P3HT:PCBM blend on higher GNF concentration modified surface and found that clusters form on

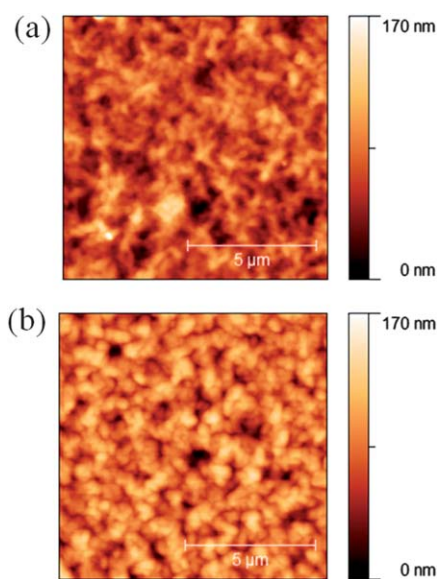


Fig. 5 AFM images of P3HT:PCBM blend on (a) ZnO-nanorods and (b) GNFs/ZnO.

the blend surface (ESI†, Fig. S4). The dependence of morphology feature on GNF concentration suggests a higher impact of GNFs on morphology than surfactants.

In a GNF-free condition, the device is of moderate performance and of a carrier mobility of $2.6 \times 10^{-4} \text{ cm}^2 \text{ V}^{-1} \text{ s}^{-1}$. By modifying the ZnO-nanorod surface with 5 mg mL^{-1} GNF solution, the performance of the device can be increased by up to 100% with an enhanced mobility value of $5 \times 10^{-4} \text{ cm}^2 \text{ V}^{-1} \text{ s}^{-1}$. Obviously, the presence of GNFs can effectively improve the device performance under such conditions. However, by further increasing the GNF concentration, the distribution of GNFs and the morphology of the corresponding upper active layer change leading to a decreased device performance (see ESI† for details). Therefore, based on the combination effects of GNFs, surfactants, and morphology, there is a trade-off among them and the optimal condition is at using 5 mg mL^{-1} GNF solution.

As the energy band diagram of the device shown in Fig. 6(a), the work function of GNFs (4.5 eV^{28}) is $\sim 0.1 \text{ eV}$ lower than the conduction band edge of ZnO-nanorods (4.4 eV). It was reported^{29,30} that the gapless GNFs can open up a gap by water and other gas molecule adsorption. Yavari *et al.*²⁹ found that the bandgap opening depends upon the humidity of the environment and the corresponding exposure time, and reaches an asymptotic value of 0.2 eV beyond a critical humidity for 2.5 h exposure. Due to the possible adsorption of water molecules on GNF surfaces during processing, a possible bandgap of $<0.2 \text{ eV}$ can open in our case as shown in Fig. 6. Electrons in the PCBM phase can be collected by travelling directly or through GNFs prior to ZnO-nanorods. Holes travel in the P3HT phase to a silver metal electrode with the possibility of being trapped at GNFs.

Additionally, spatially isolated GNFs form three-dimensional potential wells with their surrounding polymer blend for electrons transport (Fig. 6(b)) as those for ZnO-nanorods do. The GNFs and nanorods are located at the bottom of the potential wells. Because the dimensions, conductivity, and mobility of GNFs are much superior to that of semiconducting ZnO, electrons tend to hop to the highly conducting GNF surface. Electron flows in the PCBM phase favor to gather at those GNFs instead of directly moving to ZnO-nanorods. In a sense, those GNFs serve as “electron drains” to collect photogenerated electron flows and drain them out of the excess blend volume to the electrode through the underneath ZnO-nanorods as a lower resistivity pathway for electron transport. Thus, the electron transport path in the extra photoactive material is directed

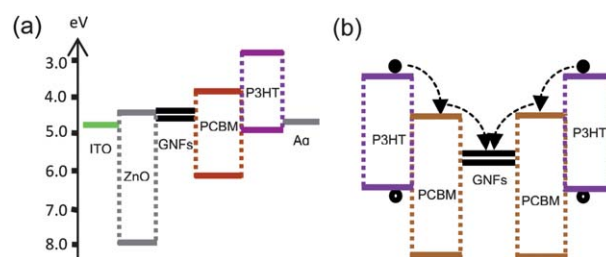


Fig. 6 Energy level alignment of the structure studied. (a) Photovoltaic device structure of ITO/ZnO/GNFs/P3HT:PCBM/Ag. (b) GNFs with the surrounding polymer blend. The bandgap opening for GNFs is $<0.2 \text{ eV}$.

through highly conducting GNFs resulting in enhanced electron mobility. The influence of enhanced electron mobility on the hole motion is reflected on the surface potential analysis.

In order to gain more insight into the impact of GNFs on the bi-carrier transport properties of the polymer blend, we employed the Kelvin probe force microscopy (KFM) measurements³¹ to probe the surface potential both in the dark and under illumination for P3HT:PCBM/ZnO (Fig. 7(a)) and P3HT:PCBM/GNFs/ZnO (Fig. 7(c)) structures. In a dark environment, both images demonstrate the local energy level alignment of P3HT:PCBM with underneath structures. Upon illumination, the photogenerated excitons dissociate at the P3HT/PCBM interfaces. Electrons migrate to the bottom ITO electrode through PCBM regions and holes diffuse toward the surface through P3HT regions. Consequently, the contrast between dark and illumination conditions is enhanced; particularly, there is a significant enhancement in the GNF-modified structure.

By analyzing the surface potential profile across photon active and de-active regimes, the values for both structures shift positively under illumination, suggesting an enlargement of the surface work function due to hole accumulation. The surface potential increments are of 30 and 90 meV for P3HT:PCBM on ZnO (Fig. 7(b)) and GNFs/ZnO (Fig. 7(d)), respectively. Higher hole concentration is driven toward the surface in contact with the silver metal electrode in the presence of GNFs. Though the energy band alignment shows the possibility of carrier recombination at GNFs, the enhanced electron mobility, *i.e.*, fast transfer of electrons from GNFs to the underneath ZnO-nanorod, reduces the electron lifetime on GNFs resulting in lowering the probability of hole capturing. As a result, the hole concentration in the P3HT phase increases and is reflected in the enlargement of the surface potential.

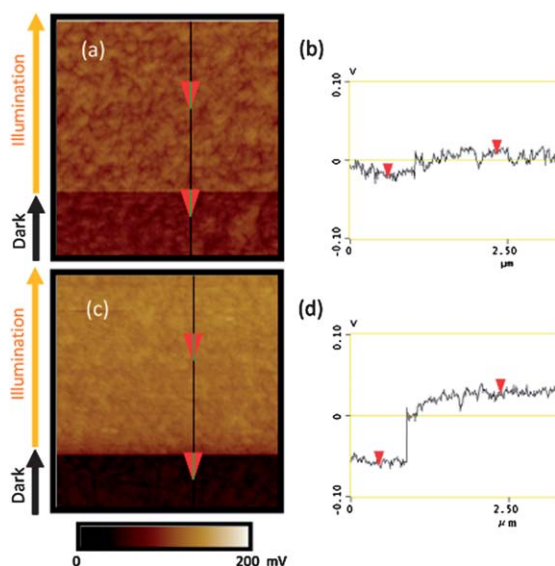


Fig. 7 Surface potential images of the P3HT:PCBM blend on (a) ZnO and (c) GNFs/ZnO structures on a $3\ \mu\text{m} \times 3\ \mu\text{m}$ surface area obtained by KFM measurements. Each image contains the result taken in the dark and under illumination as marked. The surface potential profile across the photon active and de-active regions is denoted by the straight line with two red arrows for the P3HT:PCBM blend on (b) ZnO and (d) GNFs/ZnO.

The incorporation of GNFs in inverted hybrid P3HT:PCBM/ZnO devices results in large increases in J_{SC} and V_{OC} . For the same amount of photons absorbed, there is no reduction in J_{SC} though there is $\sim 10\%$ reduction in the overall charge collection surface due to GNF arrays coverage. Thus, GNF plays a critical role in not only compensating parts of the collection surface loss, but also amplifying the collection effects. As evidenced by CELIV measurement, adding GNFs enhances the electron mobility of the device, indicating that efficient and effective electron pathways are developed in the electron transporting network. As suggested by the energy band alignment, electron pathways converge to those relatively large GNFs prior to connecting to the ordered nanorod paths. The developed pathways are of lower resistivity in transporting electrons, which in turn minimizes possible interfacial recombination events. In addition, KFM reveals that a large amount of holes move toward the surface to be extracted. As a result, free electron and hole concentrations are raised in the constituent transport phase leading to photocurrent enhancement. Hence, the space charge inside the device is reduced and the quasi-Fermi level position in each phase responds accordingly resulting in the increase in quasi-Fermi level differences. Consequently, the internal voltage drop is reduced leading to the enhanced V_{OC} . Due to partial coverage of the ZnO-nanorod growth area, GNFs decrease the direct contact probability of P3HT with the ZnO buffer layer for creating short paths through the pinholes in the buffer layer. The decrease in short paths may contribute to the enhanced V_{OC} as well.

We mention here that the performance of our GNF-modified device has not been optimized yet. Further improvement of the GNF-modified device is possible through developing good methods to solve the reaggregation problem of GNFs deposited from high concentration solutions (ESI†, Fig. S2). In addition, from the energy band diagram shown in Fig. 6, it seems that it is possible to replace the ZnO-nanorod with GNFs. However, GNFs lack the hole blocking ability of ZnO-nanorods and they should be very difficult to completely cover the underneath ITO electrode to prevent short path creation as well by current processing methods. In both cases, direct recombination of holes on the electron collection ITO electrode is highly favorable and can result in worse device performance than our standard cell.

Instead of nanorods, we have applied the GNF approach to the inverted photovoltaic device using ZnO-nanoridges. Those nanoridges are $\sim 100\ \text{nm}$ wide, $\sim 200\ \text{nm}$ thick, and $>0.5\ \mu\text{m}$ apart. GNFs are confined on the planar surface between nanoridges. We also observed similar effects of GNFs on this type of configuration. The GNF-modified cells show higher power conversion efficiency based on the moderate improvement ($\sim 10\%$) in J_{SC} and V_{OC} . Thus, the proposed approach is valid in a planar charge collection film as well.

It should be noted that the newly developed concept of using GNFs scattered on top of the electron transporting layer in inverted photovoltaic cells here can improve charge extraction efficiency quite well. The advantages of our approach include the use of a low-cost and abundant carbon resource and a simple room temperature fabrication process. Moreover, the unique properties of graphene such as high conductivity, high carrier mobility, and appropriate work function can be fully utilized. We stress that the use of graphene with nanoscale size to form spot

films is in stark contrast with that forming a continuous film used as an electrode.⁵ Our approach proposed is valid in a thick photoactive film case and should be able to be generalized to other photovoltaic cell systems using different photoactive blends or configurations as well.

Conclusions

We demonstrate an approach to assist charge extraction out of the P3HT:PCBM blend in the inverted hybrid photovoltaic cells by using GNFs. A significant improvement in device performance by up to 100% is obtained. Due to the relatively higher work function and superior electrical properties, those spatially isolated GNFs serve as electron drains for collecting and transporting photogenerated electrons. Hence, the electron transport path is modulated and is of lower resistivity, *i.e.*, higher mobility. Additionally, GNFs promote the photogenerated holes to move toward the cathode as revealed in the enlargement of the surface potential. Therefore, a large amount of photogenerated carriers can be extracted out of the photoactive material and the space charge inside the device is reduced. Consequently, the device performance is improved.

Acknowledgements

This work is supported by the National Science Council, Taiwan (Project No. NSC 98-2112-M-239-001-MY3) and Excellent Research Projects of National Taiwan University (Project No. 100 nanocenter 03).

Notes and references

- 1 A. K. Geim and K. S. Novoselov, *Nat. Mater.*, 2007, **6**, 183–191.
- 2 X. Wang, L. Zhi and K. Müllen, *Nano Lett.*, 2008, **8**, 323–327.
- 3 G. Eda, G. Fanchini and M. Chhowalla, *Nat. Nanotechnol.*, 2008, **3**, 270–274.
- 4 M. Jin, H. K. Jeong, W. J. Yu, D. J. Bae, B. R. Kang and Y. H. Lee, *J. Phys. D: Appl. Phys.*, 2009, **42**, 135109-1–135109-5.
- 5 G. Eda, Y. Y. Lin, S. Miller, C. W. Chen, W. F. Su and M. Chhowalla, *Appl. Phys. Lett.*, 2008, **92**, 233305-1–233305-3.
- 6 Q. Liu, Z. Liu, X. Zhang, N. Zhang, L. Yang, S. Yin and Y. Chen, *Appl. Phys. Lett.*, 2008, **92**, 223303-1–223303-3.
- 7 M. P. de Jong, L. J. van Ijzendoorn and M. J. A. de Voigt, *Appl. Phys. Lett.*, 2000, **77**, 2255–2257.
- 8 M. Jorgensen, K. Norrman and F. C. Krebs, *Sol. Energy Mater. Sol. Cells*, 2008, **92**, 686–714.
- 9 (a) P. Ravirajan, A. M. Peiró, M. K. Nazeeruddin, M. Grätzel, D. D. C. Bradley, J. R. Durrant and J. Nelson, *J. Phys. Chem. B*, 2006, **110**, 7635–7639; (b) C. T. Chang, F. C. Hsu, S. W. Kuan and Y. F. Chen, *Sol. Energy Mater. Sol. Cells*, 2011, **95**, 740–744.
- 10 D. C. Olson, J. Piris, R. T. Collins, S. E. Shaheen and D. S. Ginley, *Thin Solid Films*, 2006, **496**, 26–29.
- 11 C. Y. Huang, M. Y. Chou, K. H. Liu, W. H. Tsai and C. F. Lin, *Org. Electron.*, 2009, **10**, 1060–1065.
- 12 N. Sekine, C. H. Chou, W. L. Kwan and Y. Yang, *Org. Electron.*, 2009, **10**, 1473–1477.
- 13 K. Takanezawa, K. Hirota, Q.-S. Wei, K. Tajima and K. Hashimoto, *J. Phys. Chem. C*, 2007, **111**, 7218–7223.
- 14 K. M. Coakly and M. D. MaGehee, *Chem. Mater.*, 2004, **16**, 4533–4542.
- 15 C. Y. Chou, J. S. Huang, C. H. Wu, C. Y. Lee and C. F. Lin, *Sol. Energy Mater. Sol. Cells*, 2009, **93**, 1608–1612.
- 16 G. Li, V. Shrotriya, J. Huang, Y. Yao, T. Moriarty, K. Emery and Y. Yang, *Nat. Mater.*, 2005, **4**, 864–868.
- 17 M. Lotya, Y. Hernandez, P. J. King, R. J. Smith, V. Nicolosi, L. S. Karlsson, F. M. Blighe, S. De, Z. Wang, I. T. McGovern, G. S. Duesberg and J. N. Coleman, *J. Am. Chem. Soc.*, 2009, **131**, 3611–3620.
- 18 M. Ohyama, H. Kozuka and T. Yoko, *Thin Solid Films*, 1997, **306**, 78–85.
- 19 L. Vayssieres, *Adv. Mater.*, 2003, **15**, 464–466.
- 20 P. Brown, D. S. Thomas, A. Köhler, J. S. Wilson, J. S. Kim, C. M. Ramsdale, H. Sirringhaus and R. H. Friend, *Phys. Rev. B: Condens. Matter Mater. Phys.*, 2003, **67**, 064203-1–064203-16.
- 21 C. Y. Chou, J. S. Huang, C. H. Wu, C. Y. Lee and C. F. Lin, *Sol. Energy Mater. Sol. Cells*, 2009, **93**, 1608–1612.
- 22 G. Juška, K. Arlauskas, M. Viliūnas and J. Kočka, *Phys. Rev. Lett.*, 2000, **22**, 4946–4949.
- 23 A. J. Mozer, N. S. Sariciftci, A. Pivrikas, R. Österbacka, G. Juška, L. Brassat and H. Bässler, *Phys. Rev. B: Condens. Matter Mater. Phys.*, 2005, **71**, 035214-1–035214-9.
- 24 A. J. Mozer, N. S. Sariciftci, L. Lutsen, D. Vanderzande, R. Österbacka, M. Westerling and G. Juška, *Appl. Phys. Lett.*, 2005, **86**, 112104-1–112104-3.
- 25 G. Juška, N. Nekrasas, K. Arlauskas, J. Stuchlik, A. Fejfar and J. Kočka, *J. Non-Cryst. Solids*, 2004, **338–340**, 353–356.
- 26 J. Huang, G. Li and Y. Yang, *Appl. Phys. Lett.*, 2005, **87**, 112105.
- 27 A. Baumann, J. Lormann, C. Deibel and V. Dyakonov, *Appl. Phys. Lett.*, 2008, **93**, 252104-1–252104-3.
- 28 J. W. G. Wildoer, L. C. Venema, A. G. Rinzler, R. E. Smalley and C. Dekker, *Nature (London)*, 1998, **391**, 59–62.
- 29 F. Yavari, C. Kritzinger, C. Gaire, L. Song, H. Gullapalli, T. Borca-Tasciuc, P. M. Ajayan and N. Koratkar, *Small*, 2010, **6**, 2535–2538.
- 30 F. Schedin, A. K. Geim, S. V. Morozov, E. W. Hill, P. Blake, M. I. Katsnelson and K. S. Novoselov, *Nat. Mater.*, 2007, **6**, 652–655.
- 31 V. Palermo, M. Palma and P. Samori, *Adv. Mater.*, 2006, **18**, 145–164.